ACS OMEGA

Open Access

http://pubs.acs.org/journal/acsodf

Article

Supramolecular Ni(II)-Selective Gel Assembly toward Construction of a Schottky Barrier Diode

Vaishali Singh, Deepak Kumar Chauhan, and Rampal Pandey*

Cite This: *ACS Omega* 2025, 10, 378−389

Read Online

ACCESS | Metrics & More | Article Recommendations | Supporting Information

ABSTRACT: A mechanically stable and thermo-irreversible supramolecular Ni(II)-selective gel (**MG**) has been developed by utilizing the N,O-donor Schiff base (E)-1-((4-(diethylamino)phenylimino)-methyl)naphthalen-2-ol (**HL**) gelator and Et_3N in binary THF:CH_3OH (1:1) solutions at room temperature (rt). Metallogel **MG** has been characterized by spectral and analytical techniques, i.e., ESI-MS, FT-IR, NMR (^1H & ^{13}C), powder-XRD, FE-SEM, and rheological analysis. Further, noncovalent interactions responsible for the gelation mechanism have been illustrated with the aid of powder-XRD and FE-SEM analysis. The toughness, viscoelasticity, and flow behavior of **MG** were explored through rheological studies. Rheological and compressive measurements showed higher values of storage modulus and rigidity of **MG**; however, the flow property along with enrichment of toughness in **MG** can be an analytical metric for various engineering and industrial applications. Eventually, a Schottky barrier diode (SBD) was successfully constructed to mimic the functionality of **MG**-based metal−semiconductor (MS) junction devices for possible application in electrical engineering.

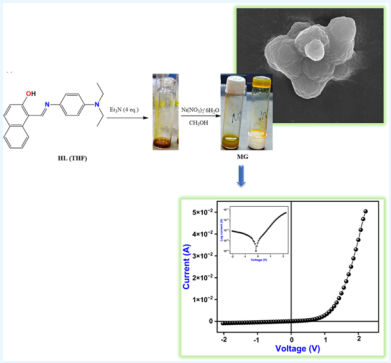

1. INTRODUCTION

Metallogel soft materials are the supramolecular assembly of small organic/inorganic molecules or low-molecular-weight gelators (LMWGs) and metal ions entrapping the protic or aprotic solvents.[1,2] LMWGs and polar/nonpolar solvents are two major components that are essential to the gelation process. LMWGs immobilize the appropriate solvent molecules to form a three-dimensional (3D) gel network. In addition, the formation of metallogel soft materials can be accomplished by introducing metal ions, thereby involving intermolecular supramolecular interactions to construct a multidimensional matrix structure.[3,4] A small variation in the design of LMWGs' molecular structure gives rise to gelation with advantageous properties and affects the morphology of the material in surprising ways.[5,6] Till date, soft materials/metallogels have been dominant over organogels[7−9] due to their physical and chemical characteristics, with potential applications in diverse areas.[10−12] The flow behavior of soft materials such as colloids,[13,14] emulsions, and suspensions[15] has engrossed significant attention in the thrust of scientific research areas.[16] Metallogels are abundant in numerous areas of applications like food, nail paints, cosmetics, toothpaste, and daycare products, while their manufacturing is strongly based on flow behavior.[17] Various LMWGs,[18,19] viz, modified amino acids, alkenes, peptides, amides, urea, carbohydrates, and sugars, can activate gelation via physical or chemical synthetic routes and form supramolecular gel scaffolds through noncovalent interactions such as H-bonding, hydrophobic, electrostatic, $\pi-\pi$ stacking, van der Waals forces, and metal coordination, which collectively contribute to the stability and formation of a 3D metallogel network.

Metallogels exhibit advantageous properties[20,21] such as solid-like,[22,23] flow dynamics, which is due to the intermolecular coupled energy[24,25] and the volume portion of the solvent molecule.[26] The application of shear flow is attributed to the liquid-like behavior and the perception of shear stress is often utilized to elaborate the phase (solid−liquid) transition.[27,28] Metallogels find widespread applications, including sensors/biosensors and actuators, drug release, tissue engineering, and drug delivery.[29−31] Nevertheless, the mechanical properties, i.e., rigidity, toughness, and crack resistance,[32−34] of the metallogels are underprivileged, which bound the performance of the gel in some applications. Formerly, some hydrogels and organogels[13,35,36] comprising toughness and mechanical strength were synthesized, but these gels limited their performance in some areas of engineering and industrial applications. In this context, the metallogel has been used to enhance the gel's mechanical strength and toughness properties,[11,33,37] whereas transition metal ions induce various remarkable functions in the gel scaffolds, including redox activity, magnetic and optical behavior, conductivity, catalysis,

Received: July 10, 2024
Revised: December 20, 2024
Accepted: December 23, 2024
Published: January 2, 2025

Scheme 1. Synthetic Representation and Molecular Structure of HL

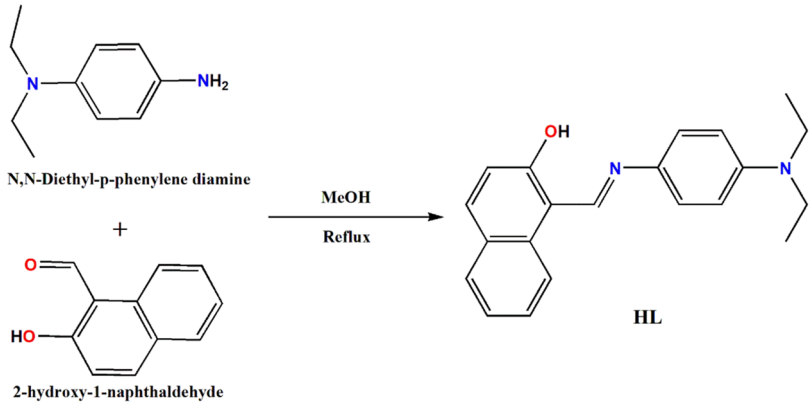

sensors, and actuators. Remarkably, metallogels that include transition metal ions [Mn(II), Fe(II/III), Co(II), Ni(II), Cu(II), Zn(II), and Cd(II)] have strong applications in various scientific fields such as chemosensors, medical diagnostics, electrochemical devices, drug delivery, catalysis, cell culturing, tissue engineering, pollutant removal, biochemistry, lithography, wound healing, fluorescent tags, electronic devices, and biomineralization.[9,18,38−40] Among these, metallogels containing Ni(II) are particularly notable for their diverse applications including fluorescence switching, electrocatalysis, nonlinear properties such as self-healing, semiconducting devices, and magnetic materials.[11,41−43] Previously, acid-based LMWGs were utilized for the formation of an Ni(II)-selective gel and were employed for semiconducting electronic devices.[43] Schottky diode-based metallogels are renowned for their tunable electronic properties, stability, versatile fabrication methods, tailored surface properties, and compatibility with other electronic components, thereby making them essential for various electronic applications requiring precise control and reliable performance. The present work entails the development of a metallogel (**MG**) constructed with the selective interaction of **HL** with Ni^{2+} ion in the presence of Et_3N base in a binary THF:CH_3OH (1:1) solvent system at rt. Nickel(II) is well known for its electrical and conductivity properties[44] due to its paramagnetic nature. Further, Ni(II)-selective **MG** leads to a flow-like structure and morphological transitions, showing a hierarchical spherical three-dimensional aggregation.[45,46] Rheological and compressive measurements indicate that Ni(II) is attributed to the rigidity and toughness of **MG**. In addition, we have successfully developed a metallogel-based Schottky barrier diode (SBD) that acts as a semiconductor (MS) junction for electronic applications in electrical devices.

2. EXPERIMENTAL SECTION

2.1. Materials. Ni(II)-gel forming chemicals such as 2-hydroxy-1-naphthaldehyde and *N*,*N*-diethyl-*p*-phenylenediamine were procured from Sigma-Aldrich Pvt. Ltd. and used as received for the gelation process. Solvents (THF/MeOH) and Et_3N were procured from HiMedia and Loba Chemie, respectively, and used without additional purification processes for Ni(II)-gel synthesis. Cadmium(II) nitrate tetrahydrate, copper(II) nitrate trihydrate, cobalt(II) nitrate hexahydrate, zinc(II) nitrate hexahydrate, and nickel(II) nitrate hexahydrate were collected and employed as received from Central Drug House (CDH).

2.2. Characterizations. ^{1}H NMR spectrum was recorded on a Bruker-400 MHz spectrometer at 400 MHz in $CDCl_3$ using $(CH_3)_3SiH$ as an internal standard. A Bruker FT-IRvertex70/80 infrared spectrometer was used to obtain the FT-IR spectra. Mass spectrometric analysis of materials was done by a Waters Synapt G2-Si Q ToF mass spectrometer. Morphological investigations were carried out through scanning electron microscopy (SEM, S3700N) of the compounds (**HL** and **MG**). Powder X-ray diffraction (PXRD) patterns were obtained by a Rigaku Ultima IV fully high-resolution X-ray diffractometer system with Cu$K\alpha$ radiation (1.54006 Å). Rheological and compressive measurements were executed on Anton Paar SmartPave SN83158100 Rheometer MCR 102 furnished with a parallel stainless-steel plate (25 mm diameter, 0.5 mm gap). For electrical characterization of the **MG** thin film device, the current−voltage (I−V) characteristics were obtained by a Keithley 2635B source meter at the corresponding applied bias voltage sequentially within the limit of ±2. All of the preparations and measurements were carried out at room temperature and under ambient conditions.

2.3. Synthesis of (E)-1-((4-(diethylamino)-phenylimino)methyl)naphthalen-2-ol (HL). The **HL** gelator[47] was synthesized by adopting a new synthetic strategy in which 2-hydroxy-1-naphthaldehyde (1 mmol) in CH_3OH (5 mL) was added dropwise to the stirring methanolic solution (5 mL) of *N*,*N*-diethyl-*p*-phenylene (1 mmol) and the reaction mixture was refluxed for 5 h. The red precipitate thus obtained after completion of the reaction was filtered and splashed with MeOH (two times) followed by diethyl ether (three times). The desired product was air-dried and recrystallized with a 1:2 ratio of solvents such as dichloromethane/diethyl ether, leading to a shiny red color crystal (Scheme 1). Yield (0.1748 g; 54.8%). Anal. Calcd [$C_{12}H_{22}N_2O$]: C 79.21; H 6.96; N 8.80; O 5.02%; Found: C 79.24; H 6.71; N 8.79; O 5.20%; ATR-FT-IR (wavenumber, cm^{-1}): 3360, 2966, 1713, 1615, 1517, 1497, 1399, 1350, 1330, 1270, 1180, 1162, 1138, 1073, 1000, 950, 803, 738, 628, 571, and 550. ^{1}H NMR ($CDCl_3$-*d*, 400 MHz) δ_H, ppm = 15.96 (s, 1*H*, −O*H*), 9.21 (s, 1*H*, −C*H*=N−), 8.02−8.00 (d, 1*H*, Ar), 7.68−7.65 (d, 1*H*, Ar), 7.44−7.40 (m, 1*H*, Ar), 7.25 (s, 1*H*, Ar), 7.22−7.21 (d, 2*H*, Ar), 7.02−7.00 (d, 1*H*, Ar), 6.67−6.65 (d, 2*H*, Ar), 3.36−3.30 (m, 4*H*, −CH_2), 1.15−1.11 (t, 6*H*, −CH_3).^{13}C NMR ($CDCl_3$-*d*, 125 MHz) δ_C, ppm = 160.1, 158.8, 148.1, 142.7, 135.1, 132.4, 129.1, 128.0, 126.8, 126.6, 123.9, 123.2, 118.4, 115.6, 108.6, 44.7, and 13.0. ESI-HRMS (m/z) for

https://doi.org/10.1021/acsomega.4c06387
ACS Omega 2025, 10, 378−389

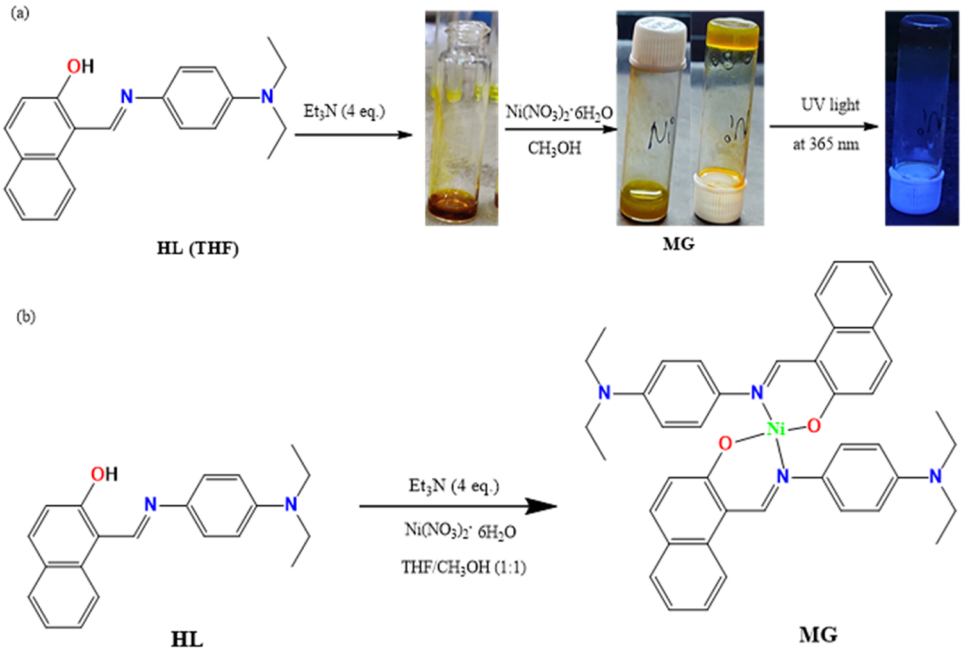

Figure 1. (a) General representation of **HL** (THF) with alcoholic Ni(II) ion solution in the presence of a base (Et_3N, 4 equiv) to the formed Ni(II)-selective gel (**MG**). (b) Molecular structure and synthesis procedure of Ni(II)-selective gel (**MG**).

$C_{12}H_{22}N_2O$: Calculated $[M]^+$: 318.1732; Found $[M]^+$: 318.1766.

2.4. Synthesis of Ni(II)-metallogel (MG). The **MG** was instantaneously formed through direct mixing of a methanolic solution (500 μL) of $Ni(NO_3)_2{\cdot}6H_2O$ (0.0125 mmol) into a clear THF solution (500 μL) of **HL** (CGC ~8 mg, 0.025 mmol) in the presence of TEA (0.2 mmol, 4 equiv) at rt. A translucent and green stiff gel was obtained with one stroke of shaking and commonly examined by the "inverted glass vials" test (Figure 1). FT-IR (cm^{-1}): 3400, 3040, 2987, 2770, 2709, 2534, 1628, 1450, 1300, 1167, 1040, 824, 779, 624, and 546. ESI-HRMS (m/z) for $C_{42}H_{42}N_4NiO_2$: Calculated $[M]^+$: 692.2661; Found $[M]^+$: 693.2853.

3. RESULTS AND DISCUSSION

The bidentate N,O-donor Schiff base **HL** gelator was synthesized by a condensation reaction involving a methanolic solution of 2-hydroxy-1-naphthaldehyde and *N*,*N*-diethyl-*p*-phenylenediamine in an equimolar ratio (1:1) at refluxing conditions (Scheme 1). The resultant red color powder **HL** was soluble in aprotic solvents and insoluble in other protic solvents (Table S1). Further, a red precipitate of **HL** was recrystallized with dichloromethane (DCM) solvent and red shiny crystals were obtained.

3.1. Spectral Characterization of the Gelator. Different spectral techniques such as ^{1}H NMR and FT-IR have been used for the characterization of the **HL** gelator. ^{1}H NMR analysis of **HL** exhibits a sharp singlet peak for azomethine (−CH═N−)[48] proton at 9.21 ppm along with a broad signal for phenolic −OH proton[47] at 15.96 ppm due to the existence of intramolecular hydrogen bonding interaction.[49] Protons of the aromatic ring show signals in the range of ~6.67−8.02 ppm and also display multiplet signals for aliphatic $-CH_2$ protons in the region of 3.32−3.03 ppm. The resonance of the aliphatic $-CH_3$ groups of diethyl groups appeared as a triplet in the region of ~1.15−1.11 ppm and established the formation of the gelator **HL** (Figure S1). The FT-IR spectrum for the **HL** gelator depicts several symmetric and asymmetric broad bands for phenolic groups (−OH, stretching) at 3360 cm^{-1} and for aliphatic groups (−CH, stretching) at 2966 cm^{-1}. A significant band for the azomethine group (C═N, sharp) appeared at 1615 cm^{-1}, which is well related to a strong sharp band for C−O and C−N groups at 1399 and 1350 cm^{-1}, respectively. Also, characteristic sharp vibrations were observed in the range of 1500−1000 cm^{-1} for the aromatic ring (C═C, bending), which displays the formation of the functional bidentate Schiff base **HL** gelator (Figure S2).

3.2. Gelation Study. The naphthol-based Schiff Base[50,51] gelator **HL** contains an N,O-donor active site that exhibits excellent solubility in aprotic solvents together with hydrophobic and hydrophilic groups. These groups can construct a suitable aggregation/binding of small molecules, thereby establishing the supramolecular gel assembly of **HL**.[28,52] Different possibilities were inspected to know its gelation behavior; however, no gelation was observed in an aprotic solvent or mixture of aprotic solvents. The basic medium in the presence of Et_3N and nitrate salts of transition metal ions (Cd^{2+}, Zn^{2+}, Cu^{2+}, Ni^{2+}, Co^{2+}, Fe^{2+}, and Mn^{2+}) was induced into the THF solution of **HL** for envisaging the scaffolding of the supramolecular gel (Figure S3). The green color transparent **MG** was instantly formed upon adding a methanolic solution of Ni(II) to a THF solution of **HL** under a basic medium at rt without any external forces such as heating, cooling, and sonication (Figure 1a). The optimization of gelation was found selectively with Ni(II), leading to the stable and transparent **MG** when incorporated into a basic medium of a THF-MeOH mixture comprising **HL** (Figure S3). The basic medium was essential for the formation of the gel, as under neutral conditions the addition of Ni(II) to **HL** solution results in a clear solution, which may be attributed to the deprotonation of the phenolic −OH group in **HL**. The triethylamine (Et_3N) as base was used to trigger the gelation process in **HL**, which augmented the hydrophobicity[53] in the molecule and increased the formation of **MG** with Ni(II)

https://doi.org/10.1021/acsomega.4c06387
ACS Omega 2025, 10, 378−389

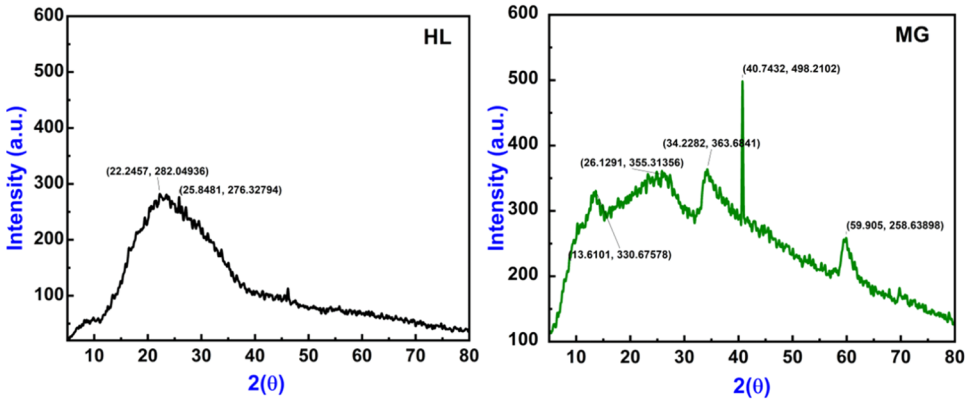

Figure 2. Powder-XRD pattern of **HL** (left) and **MG** (right).

ion.[28,52] In addition, the effect of the counteranion was also determined by using $NiCl_2$ salt under optimized conditions; it was observed that it forms an Ni(II)-selective gel (**MG**). It is envisaged that the counteranions of metal salts (Cl^- and NO_3^{2-}) have an insignificant effect on forming the supramolecular assembly. The gel assembly with the Cl^- anion of Ni(II) also formed a stable and green color translucent gel and after evaporation of solvents, it converted into a dark green solid (Figure S4). Specifically, the presence of Ni(II) in MeOH under the basic media of **HL** leads to the formation of **MG** by involving noncovalent interactions. The instant formation of **MG** exhibits a fast kinetics of Ni(II)-**HL** coordination and results in the aggregation of the supramolecular assembly formation via noncovalent interactions (Figure 1b).[54,55] Furthermore, the gelation ability of **HL** was investigated in different solvents under similar conditions. The solubility of **HL** was also tested in aprotic solvents such as acetone, chloroform, dichloromethane, DMF, DMSO, 1,4-dioxane, and THF (Table S1). The binary mixture of THF:MeOH and 1,4-dioxane:MeOH solvents leads to instant gelation selectively with Ni(II) in the presence of Et_3N (4 equiv); other mixtures of solvents did not show gelation under similar conditions (Figure S5). Furthermore, the binary mixture of THF:MeOH solvents was more mechanically stable than that of 1,4-dioxane:MeOH solvents for the formation of **MG**.

3.3. Minimum Gel Concentration. Nickel salts such as $Ni(NO_3)_2{\cdot}6H_2O$ formed the green metallogel **MG** by mixing the basic solutions of the **HL** gelator with Ni(II) in a 2:1 (**HL**:Ni^{2+}) molar ratio at rt. The optimized minimum gelation concentration[13,56] of the **HL** gelator was determined to be 0.025 mmol/mL, below which gel formation was not observed in the THF solvent. **MG** was stable, self-standing, and visible by a simple test[57] of "vial inversion" (Figure 1a).

3.4. Phase Transition Temperature. **MG** was thermo-irreversible and exhibited thermotropic behavior; the phase transition (gel−solid) temperature (T_{gel}) was ≤60 °C.[44,58] **MG** was thermally stable due to the involvement of THF-MeOH solvent molecules in the formation of the supramolecular gel matrix. When external stimuli such as heating/temperature are used, the solvent molecules are lost and converted into isotropic solids of **MG**.

3.5. Characterization of Gel Material. Metallogel **MG** was thoroughly characterized with different spectroscopic, microscopic, and analytical techniques such as Fourier-transform infrared radiation (FT-IR), electrospray ionization-high-resolution mass spectrometry (ESI-HRMS), powder X-ray diffraction (PXRD), scanning electron microscopy (SEM), and rheological investigations.

3.6. Mass (ESI-HRMS) Analysis. As mentioned above, **HL** formed a stable Ni(II)-selective gel (**MG**) in the presence of Ni^{2+} ions, which was also well corroborated by mass (ESI-HRMS) analysis. In the ESI-HRMS (in positive mode) spectrum, **MG** exhibits a significant ion peak at 692.2853 $[M]^+$ and is also interrelated with a significant peak observed at 711.1718 $[M + H]^+ + [2H_2O]$ with an empirical formula of $C_{42}H_{42}N_4NiO_2$ (Figure S6). This indicates that the formation of the Ni^{2+} ion binds with the **HL** gelator to form a supramolecular assembly of Ni(II)-selective gel (**MG**) with a 2:1 (**HL**:Ni^{2+}) molar ratio (Figure 1b). Based on the ESI-HRMS data, **HL** acts like a N,O-donor bidentate gelator that binds with the Ni^{2+} ion and solvent molecules to form a supramolecular assembly via noncovalent interactions involving metal−gelator (M−L) coordination, $\pi-\pi$ stacking, and H-bonding of **MG**.

3.7. FT-IR Analysis. Analysis of the FT-IR spectrum of **HL** revealed the characteristic bands at 3360 and 2966 cm^{-1} corresponding to phenolic (O−H) and aliphatic (C−H) groups stretching, respectively (Figure S2). Compared with the **HL** spectrum, **MG** displays a strong broad vibration for the solvent molecule (O−H) at 3400 cm^{-1} and a weak broad vibration for alkane (C−H) at 2987 cm^{-1} resembling the intramolecular hydrogen interactions with the entrapped methanol (−OH) molecule that are involved in the formation of the gel assembly (Figure S7). The vibration of imines (C═N) displays a significant band at 1628 cm^{-1} and is well corroborated with the C−O/C−N groups exhibited at 1450 cm^{-1}/1300 cm^{-1} that slightly shifted toward the higher-frequency region, which may be ascribed to Ni(II) binding with **HL** through the N,O-coordination site. Moreover, there was a wide-ranging broadening observed in the 1700−1500 and 1000−500 cm^{-1} vibration regions due to the entrapment of solvent molecules into the gel assembly of **MG**. However, substantial changes were observed in the FT-IR spectra of **MG** compared with those of **HL**, suggesting the development of an Ni(II)-selective gel (Figure S7).

3.8. ^{1}H NMR Analysis. The NMR spectrum of xerogel **MG** does not show the broad resonance at 15.96 ppm assigned to the phenolic −OH proton that supports the coordination of Ni(II) with the N,O-donor site of **HL** (Figures S8 and S1). Additionally, the aldimine (−CH═N) proton exhibits a downfield shift at 9.66 ppm and aliphatic ($-CH_2$ and CH_3) protons are upfield shifted, thereby suggesting the coordination

https://doi.org/10.1021/acsomega.4c06387
ACS Omega 2025, 10, 378−389

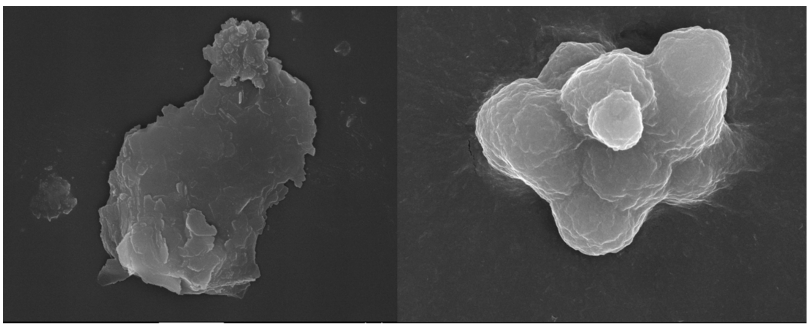

Figure 3. SEM images of **HL** (left) and **MG** (right).

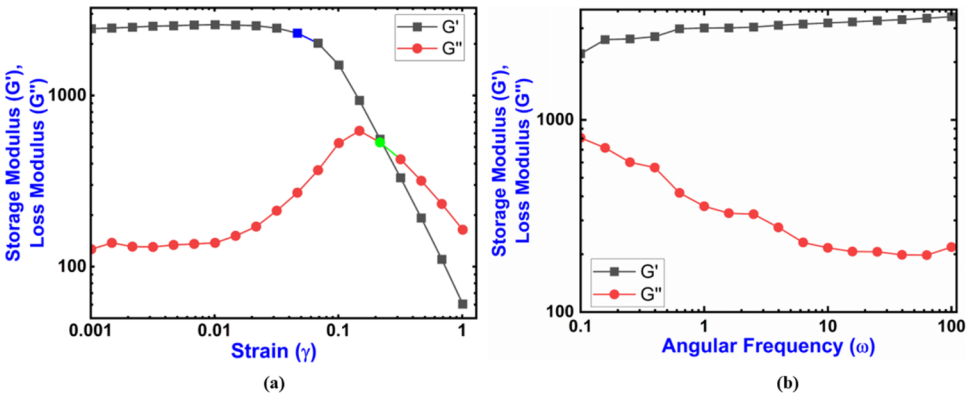

Figure 4. Rheological investigations of **MG**. (a) Amplitude-sweep measurements with LVER range 0.05%. (b) Frequency-sweep measurements at 0.05% shear strain.

between **HL** and Ni(II) due to the formation of **MG** in 2:1 molar ratio (Figure S8).

3.9. Structural Investigation. To achieve deep insights, the structural features of the vacuum-dried xerogel **MG** were compared with the **HL** acquired PXRD patterns in the 2θ range of 10−80° (Figure 2). The PXRD pattern showed significant and broad peaks of **HL** at 2θ = 22.24° and 25.84°, whereas the xerogel **MG** also exhibited broad peaks that were dissimilar from the **HL** pattern. However, **MG** displayed significant peaks at 2θ = 13.61, 26.12, 34.22, 40.74, and 59.90° (Figure 2). In addition, **MG** demonstrated a broad peak due to the large volume of solvent (MeOH) molecules entrapped inside the gel matrix. **HL** showed a peak at 2θ = 22.24° with a corresponding *d*-spacing value of 4.02 Å assignable to the existence of $\pi-\pi$ interactions,[59,60] but incorporation of Ni^{2+} exposed the shift in peak intensity at 2θ = 26.12° with the corresponding *d*-spacing value at 4.29 Å in **MG**,[28] which indicates the disruption of $\pi-\pi$ stacking. The *d*-spacing value calculated distance of 2.27 Å related to the diffraction peak at 2θ = 40.74° suggests the existence of Ni(II) ion in **MG**.[61] The PXRD pattern revealed that the Ni^{2+} ion had a noticeable effect on the binding modes to form a supramolecular assembly of **MG**. Also, the diffraction peak at 2θ = 34.22° with a *d*-spacing value of 2.74 Å retained the occurrence of the H-bonding interaction in **MG**.[62,63] Overall, the diffraction pattern (Figure 2) shows the existence of $\pi-\pi$ stacking, extensive H-bonding, immobilization of solvent molecules, and mode of metal−gelator binding responsible for the agglomerations of **MG** (Figure S9).

3.10. Morphological Investigation. Scanning electron microscopy (SEM) analysis is a reliable and useful technique to gain visual insights into the microstructure and morphology of the compound. Therefore, SEM analysis was utilized to envisage the actual microassembly structures[64,65] of **HL** and **MG** (dried xerogel). **HL** revealed an earth crust-like structure with a nonmesoscopic assembly of approximately ∼2 μm average size (Figure 3), but, in addition to Ni^{2+}, it showed a significant change in the morphology of **MG**. Immobilization of the solvent and the presence of Ni^{2+} ion in **MG** exposed the spherical-like three-dimensional structure of approximately ∼1 μm with high compactness, in which the earth crust-like structure of **HL** assembly interacts with the Ni(II) ion and eventually traps a large volume of solvent in its cavity/spaces to give a compact mesoscopic morphology[58,59] of **MG** (Figure 3). Overall, the morphology variation indicates that the assembly of **HL** interacts with the Ni(II) ion and entraps the solvent via noncovalent interactions to form the three-dimensional supramolecular assembly of **MG** (Figure 3).

In the energy-dispersive X-ray (EDX) pattern and mapping of **MG**, the presence of Ni, C, N, and O as key constitutional elements of the hybrid gel material is confirmed (Figure S10).[66] Based on mass analysis, the empirical formula is $C_{42}H_{42}N_4NiO_2$; the elemental mapping of **MG** (dried xerogel) is also well connected, illustrating the quantitative weight (%) analysis of Ni, C, O, and N constitutional elements (Figure S10) and is responsible for the presence of Ni(II) ion and **HL** gelator to form the supramolecular assembly of the Ni(II)-selective gel (**MG**).

3.11. Rheological Investigation. Compressive measurements demonstrate the thermal and mechanical strength of **MG**.[67] The measurements were executed over instantly prepared **MG** and examined by rheological studies,[27] which showed its viscoelastic property. Initially, sweep measurements (amplitude-sweep and frequency-sweep)[68] were performed to

https://doi.org/10.1021/acsomega.4c06387
ACS Omega 2025, 10, 378−389

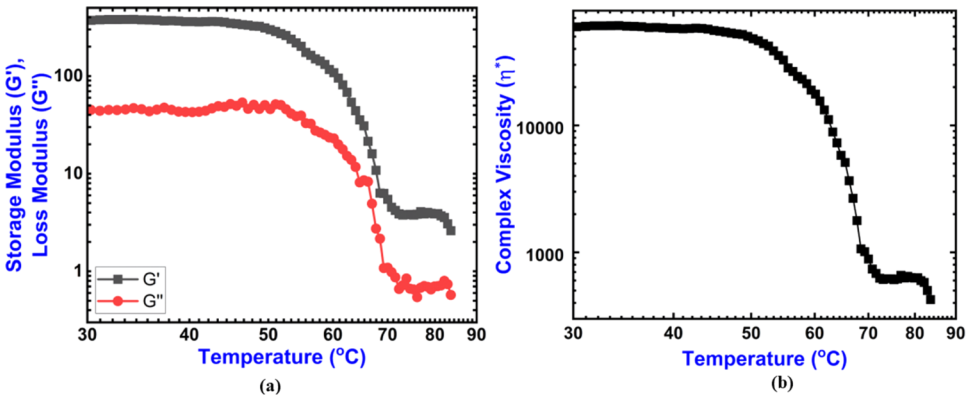

Figure 5. (a) G' and G'' vs dynamic temperature at a scan rate of 5 °C/min with 0.05% shear strain. (b) Complex viscosity vs temperature ramp tests at 5 °C/min point at critical temperatures (T_{gel}) ≤ 60 °C for **MG**.

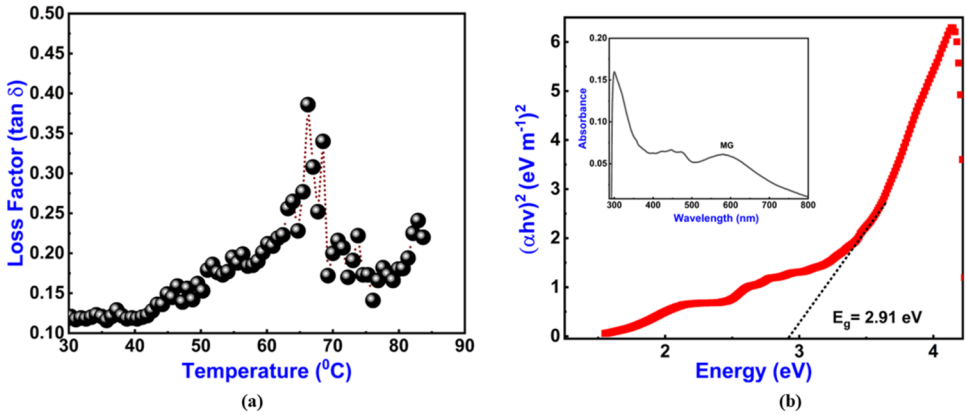

Figure 6. (a) Temperature ramp vs loss factor (tan δ) specifies T_{gel} ≤ 60 °C for **MG**. (b) UV/vis spectrum (inset) and Tauc's plot of the synthesized **MG**.

examine the elastic behavior of **MG**. In amplitude-sweep measurements, the storage modulus (G') reveals the elastic modulus, which indicates the elastic behavior, whereas the loss modulus (G'') shows the viscous modulus, which describes the flow behavior, thus showing the features of a semisolid/liquid (gel).[69] To understand the toughness and rigidity of **MG** with shear strain in the range of 0.001−1%, the amplitude-sweep experiment was executed, in which the values of G' and G'' were computed and G' displayed a high value compared to G'' at 25 °C (Figure 4a).[70] **MG** displays a G' value (>10^3) that is higher than the G'' value (>10^2) with a crossover point obtained at 0.2 shear strain showing the phase transition (gel−sol) of **MG**. The linear viscoelastic region (LVER) proposal[71] with 0.05% shear strain shows a higher G' value than G''; these ($G' > G''$) measurements show the real nature of **MG** in gel state. The measurements also display a linear LVER region at 0.05% shear strain after the distortion of the gel assembly occurs, which indicates that on increasing the strain value, the stable gelation of **MG** is lost to liquefication. The linearity of the value of shear strain from 10^{-3} to 10^{-1} implies that **MG** displays rigidity and stiffness (Figure 4a).[5]

To understand more about the rigidity or mechanical stability of **MG** at a constant strain of 0.05%, the frequency-sweep measurement[68] was conducted from 0.1 to 100 rad s^{-1} angular frequency (ω) at 25 °C.[72] This measurement also illustrates a storage modulus (G') higher than a loss modulus (G'') with the increasing value of ω, displaying the viscoelastic nature of **MG**. It also demonstrates the linear upsurge in G' and G'' values, with no deviation point obtained in the linearity, and they remained positive in the entire sweep range, which shows the rigidity and mechanical stability of **MG** (Figure 4b).[73]

Furthermore, to determine the thermal strength and temperature response on **MG**, temperature ramp measurements were performed in the range of 30−90 °C, and it was observed that the values of G' and G'' remained unaffected up to 50 °C. Nevertheless, on increasing the temperature, there was an inclination in the values of G' and G'', revealing the thermal strength of **MG** up to approximately 60 °C, and thereafter it liquefied/solidified or evaporation of the solvent occurred from the gel matrix. Thus, the critical temperature of **MG** is observed to be ≤60 °C and this rheological data analysis strongly suggests the viscoelastic nature of **MG** (Figure 5a).[74]

The temperature measurements of **MG** indicate that the phase (gel−liquid/solid) transition occurs at nearly ≤60 °C, which evidently points to gel formation using the combination of THF-CH_3OH solvents since the boiling point of oxolane and CH_3OH is 66 and 64.7 °C, respectively. The complex viscosity[75] vs temperature ramp plot shows linearity up to 50 °C, which indicates the high viscous nature and toughness of **MG**, but increasing the temperature shows a deviation in linearity as well as a phase (gel-to-liquid/solid) transition process (Figure 5b). In the measurements of temperature vs loss factor (tan δ) (Figure 6a), the calculated tan δ value was 0.30 (<1) at T_{gel} ≤ 60 °C and displayed a semi-liquid state of

https://doi.org/10.1021/acsomega.4c06387
ACS Omega 2025, 10, 378−389

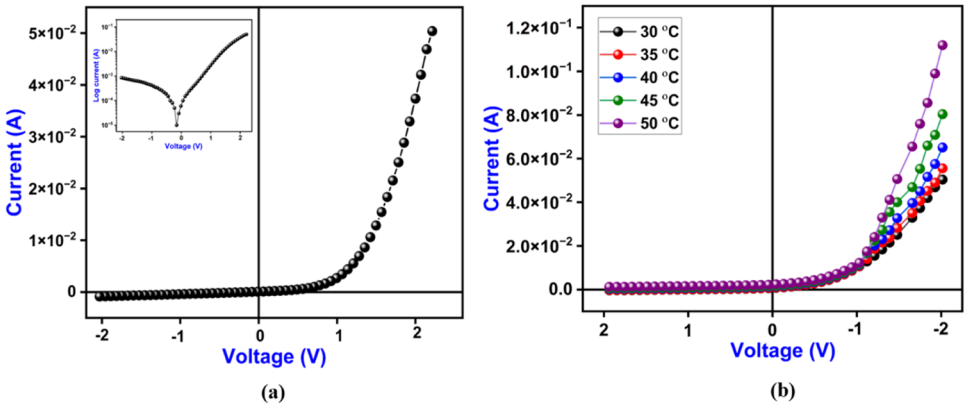

Figure 7. (a) $I-V$ and log $I-V$ (inset) curve for the synthesized ITO/**MG**/Al-based thin film device at room temperature. (b) $I-V$ curve for the synthesized ITO/**MG**/Al-based thin film device at various temperature.

MG. Overall, the above compressive experiments show the viscous nature and toughness of **MG**.[72,76]

3.12. UV/vis Spectroscopic Analysis. To determine the interaction between **HL** and Ni(II) for the formation of **MG**, the absorption spectrum of **HL** and **MG** was recorded through a UV/vis spectrometer. In the solution phase, the gelator **HL** (10 μM, THF) shows a low-energy (LE) broad band at 421 nm and high-energy (HE) band at 320 nm, which may be attributed to n $\rightarrow$ π^* and $\pi \rightarrow \pi^*$ transitions.[77−79] Moreover, the xerogel of **MG** (10 μM, THF) also displays an LE band at 580 nm (ΔE, 6512 cm^{-1}) and HE band at 300 nm (ΔE, 2083 cm^{-1}), which may be designated to n $\rightarrow$ π^* and $\pi \rightarrow \pi^*$ transitions[80,81] (Figure S11). Incorporation of Ni(II) while forming the Ni(II)-**HL** coordination complex of **MG** leads to the bathochromically shifted absorption at 580 nm and hypsochromic shift at 300 nm in absorption wavelength. Relative to **HL**, the absorption spectrum of **MG** exhibits significant changes in the wavelength, thereby indicating the metal-**HL** gelator interaction to form the supramolecular assembly of **MG** (Figure S11a). To get deeper insights, the interaction mechanism between the **HL** gelator and Ni(II) was analyzed and Job plot analysis was carried out, which endorsed 2:1 stoichiometry between the **HL** gelator and Ni^{2+} to form the supramolecular gel (Figure S11b).

3.13. Device Fabrication. Multiple metal−semiconductor (MS) junction devices have been fabricated in indium tin oxide (ITO)/**MG**/Al sandwich structure to perform electrical studies. The thin film of synthesized **MG** was deposited on a precleaned ITO-coated glass substrate. Initially, to produce an active thin film layer of **MG** slurry in the binary mixture of THF and deionized water, the **MG** xerogel was mixed and stirred at room temperature and then deposited on the top of ITO-coated glass. The thickness of the fabricated film was estimated at ∼1 μM and by thermal deposition of metal mask, an aluminum (Al) electrode was placed onto the active layer of the **MG** film under high-vacuum conditions (10^{-5} Torr) in the effective area of 7.066×10^{-6} m^2.

3.14. Optical Characterization. UV/vis analysis was executed to determine the optical property of synthesized **MG** in the solid state in the range 250−800 nm (inset; Figure 6b). In the UV/vis spectrum, the fundamental absorption corresponds to the electron that was used to evaluate the band gap of synthesized **MG**. The direct optical band gap of **MG** was calculated by Tauc's equation

$$(\propto h\nu)^n = A(h\nu - E_g) \quad (1)$$

where $\propto$, h, ν, and E_g stand for the absorption coefficient, Planck's constant, frequency of light, and optical band gap, respectively; A is a constant and is considered as unity for the ideal case. To compute the direct optical band gap, the value of the exponent of "n" in the above equation was considered as 2. By extrapolating the linear region of the plot $(\propto h\nu)^2$ vs $h\nu$ (Figure 6b) to $\propto = 0$ absorption, the value of the direct optical band gap (E_g) was estimated as 2.91 eV for **MG**.

3.15. Electrical Characterization. The calculated optical band gap of **MG** suggests its semiconductor material behavior. Therefore, a metal−semiconductor (MS) junction-based thin film device was fabricated by using ITO/**MG**/Al and their electrical parameters were inspected by analyzing the charge transport mechanism. The $I-V$ plot of the **MG** device was obtained at an applied bias voltage within the limit of ±2 V (Figure 7a). The electrical conductivity of the **MG**-based thin film device was determined to be 4.12×10^{-3} S m^{-1}, illustrative of a semiconductor material. Furthermore, the $I-V$ characteristic curve of the **MG**-based thin film device displays a nonlinear rectifying nature that is analogous to the Schottky barrier diode (SBD). The rectification ratio (I_{on}/I_{off}) of the **MG**-based SBD at ±2 V was obtained to be 58.6, which is a crucial characteristic of a material that can be employed in photovoltaic applications.

To determine the thermal stability of our fabricated **MG**-based SBD, we studied the $I-V$ characteristics of our device at various temperatures from 30 to 50 °C (Figure 7b). The $I-V$ characteristics curve for (ITO)/**MG**/Al-structured thin film devices at different temperature[82] (Figure 7b) illustrates a gradual improvement in current with an increase in temperature. The $I-V$ curves display the nonlinear rectifying signature of Schottky diodes and the device is stable up to 50 °C (Figure 7b).

The $I-V$ characteristics curve of **MG**-based SBD, further analyzed through thermionic emission theory and Cheung's method, was extracted to calculate the important diode parameters at room temperature. Primarily, the $I-V$ characteristics curve was analyzed through the following standard equations

$$I = I_0 \exp\left(\frac{qV}{\eta RT}\right)\left[1 - \exp\left(-\frac{qV}{\eta RT}\right)\right] \quad (2)$$

https://doi.org/10.1021/acsomega.4c06387
ACS Omega 2025, 10, 378−389

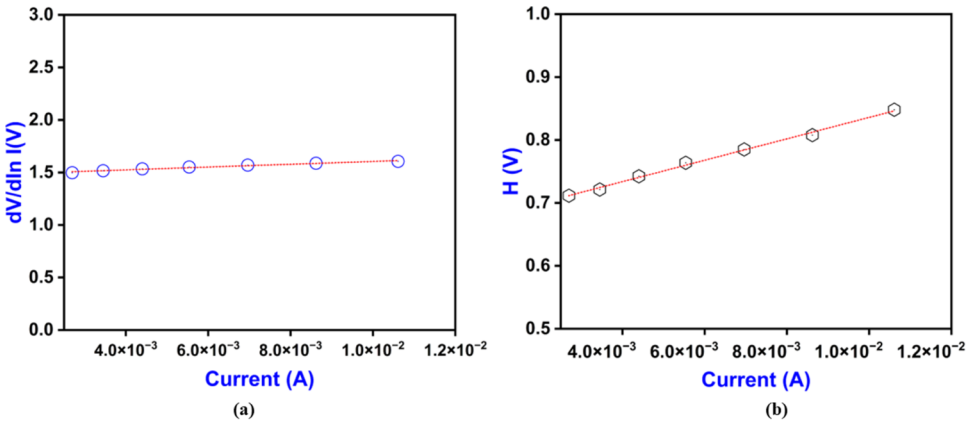

Figure 8. (a) dV/d ln I vs I and (b) H vs I for the **MG**-based thin film device.

$$I_0 = AA^*T^2 \exp\left(-\frac{q\phi_B}{KT}\right) \tag{3}$$

where I_0, q, K, T, V, A, η, and A^* represent the reverse saturation current, electronic charge, Boltzmann constant, temperature in Kelvin, forward bias voltage, effective diode area, ideality factor, and effective Richardson constant, respectively. The effective diode area was estimated to be 7.066×10^{-6} m^2 and the effective Richardson constant was 32 AK^{-2} cm^{-2} for the synthesized **MG** device.

In addition, the series resistance (R_S), ideality factor (η), and barrier potential height (ϕ_B) were calculated by using the extracted Cheung's idea equations (eqs 4−6)

$$\frac{dV}{d(\ln I)} = \left(\frac{\eta KT}{q}\right) + IR_S \tag{4}$$

$$H(I) = V - \left(\frac{\eta KT}{q}\right)\ln\left(\frac{I}{AA^*T^2}\right) \tag{5}$$

$$H(I) = IR_S + \eta\phi_B \tag{6}$$

From Figure 8a, the intercept of dV/d ln I (eq 4) plot gives us the value of η and the slope of the plot provides the R_S. The obtained value η was estimated to be 1.47, depicting that the developed MS junction is nearly close to the ideal value. The deviation from ideal behavior in MS junctions, particularly observed in Schottky diodes, is due to the existence of inhomogeneities in the Schottky barrier height, interface states, and series resistance at the junction. The barrier potential height (ϕ_B) was determined to be 0.66 eV as obtained from the intercept of H vs I, and it was found to be a substantial value for SBD (Figure 8b) by using the value of the ideality factor (η) in eq 6. The value of series resistance R_S was estimated from the slope of dV/d ln I and H vs I plot by using eqs 4 and 6 (Figure 8). The calculated series resistance (R_S), ideality factor (η), and barrier potential height (ϕ_B) for the MG-based SBD MS junction are illustrated in Table 1. The obtained parameters for **MG**-based SBD exhibited a carrier combination at the interface, which is a better barrier height, indicating its potential application in the field of semiconductor/optoelectronic devices.

To gain a comprehensive understanding of the charge transport phenomena at the MS junction, a detailed analysis of I−V curves is necessary. The characteristics of the I−V slope curve in the logarithmic scale (log current vs log voltage)

Table 1. Schottky Device Parameters of MG-based SBD

					series resistance (Ω)	
device	on/off ratio	conductivity (S m^{-1})	ideality factor	barrier height (eV)	dV/d ln I vs I graph	H vs I graph
MG	58.6	4.2×10^{-3}	1.47	0.66	133.7	170.2

illustrate two different regimes (Region I and Region II) with erratic slopes for the **MG**-based thin film device (Figure 9a). Region I represents the value of the slope close to 1, which follows the relation $I \alpha V$, indicating the ohmic regime. Region II shows the value of slope close to 2, which follows the relation $I \alpha V^2$, indicating a regime trapped with free space and dominated by space charge limited current (SCLC). In this region, injected carriers are more than background carriers and are spread over the entire region as well as generate a space charge field. The currents are regulated by this space charge field and are referred to as the SCLC theory. This theory has gained popularity and is adopted to estimate the mobility of materials in this regime (Figure 9a).

In the SCLC model, the effective carrier mobility (μ_{eff}) was determined from the higher voltage data of I vs V^2 curve (Figure 9b) by using the below Mott−Gurney equation

$$I = \frac{9\mu_{eff}\epsilon_0\epsilon_r A}{8}\left(\frac{V^2}{d^3}\right) \tag{7}$$

where I, μ_{eff}, ϵ_0, and ϵ_r stand for the current, effective carrier mobility, the permittivity of free space, and the relative dielectric constant of synthesized **MG**, respectively. The relative dielectric constant was determined by plotting the capacitance of **MG** against frequency in the film format at a constant bias potential as shown in Figure 10. The dielectric permittivity of **MG** was calculated by analyzing the saturated values of capacitance in the higher-frequency regime (Figure 10) using the following equation

$$\epsilon_r = \frac{1}{\epsilon_0}\cdot\frac{Cd}{A} \tag{8}$$

where C, d, and A represent the capacitance (at saturation), thickness of the film (∼1 μM), and effective area, respectively. The relative dielectric constant of **MG** was determined to be 1.98 by using the above formula.

To determine the charge transport across the junction, key parameters like the transit time (τ) and diffusion length (L_D)

https://doi.org/10.1021/acsomega.4c06387
ACS Omega 2025, 10, 378−389

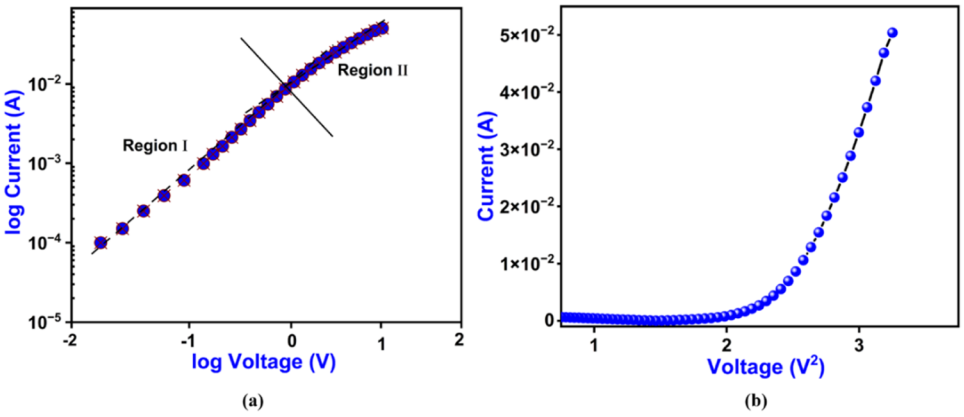

Figure 9. (a) log I vs log V curve and (b) I vs V^2 curve for the **MG**-based thin film device.

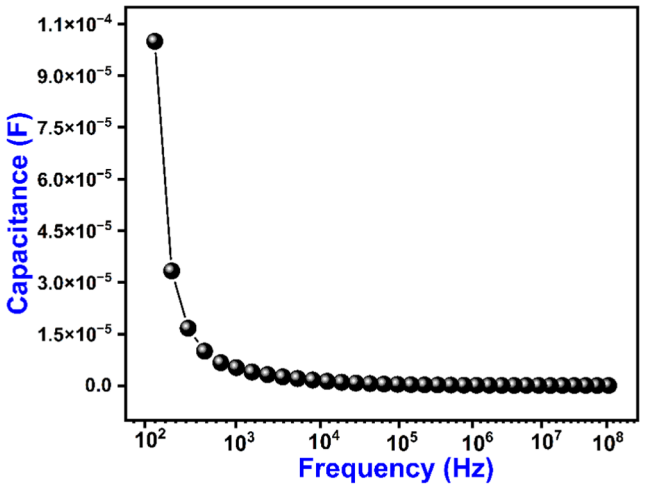

Figure 10. To determine the dielectric constant the plot of capacitance vs frequency.

were also calculated. The value of τ was estimated using eq 9 and the slope of the SCLC regime (region II) in the logarithmic illustration of the forward I–V curve (Figure 9a).

$$\tau = \frac{9\epsilon_o\epsilon_r A}{8d}\left(\frac{V}{I}\right) \quad (9)$$

$$\mu_{\text{eff}} = \frac{qD}{KT} \quad (10)$$

$$L_D = \sqrt{2D\tau} \quad (11)$$

where D stands for the diffusion coefficient and was calculated by Einstein–Smoluchowski equation, eq 10. The diffusion length L_D of charge carriers influences the device performance when the metal–semiconductor (MS) junction is formed and is further extracted from eq 11. The charge transport parameters of **MG**-based SBD are displayed in Table 2.

Higher mobility indicates a better transport rate, which illustrates the production of a higher number of charge carriers, whereas diffusion length indicates the path length of charge carriers before recombination. The **MG**-based SBD exhibits promising diode parameters, indicating the potential of these materials for promising future device applications. The donor–acceptor balance of Ni(II) centers coupled with **HL** units is a key accountable factor of the gel and may be critical for the semiconducting property of the Ni(II)-selective gel (**MG**). The **MG**-based SBD demonstrates significant device performance, with some charge transport parameters surpassing previously reported values.[82−85] Comparing these parameters with other reported values[43,86,87] indicates that **MG** can be a promising candidate for semiconducting device applications,[88,89] as shown in Table 3.

Table 3. Comparison of the Electrical Parameters of MG-based SBD Compared with Other Reported Results

device	electrical conductivity	barrier height	ideality factor	ref
Mg@MEA	1.45×10^{-5}	1.89	0.38	87
CdA-OX	5.35×10^{-4}	1.8	0.32	86
Co-TA	4.75×10^{-6}	0.76	2.38	83
Cu-TA	7.49×10^{-5}	0.36	1.65	84
Ag/Cu-H_4L	3.80×10^{-6}	0.61	3.0	85
Tb-OX	3.54×10^{-5}	0.27	1.21	87
Mn-TA	2.71×10^{-5}	0.73	1.71	88
Fe@TETA	1.003×10^{-4}	0.28	1.39	89
Ni-D-TA	5.13×10^{-5}	0.28	1.47	43
MG	4.2×10^{-3}	0.66	1.47	present work

4. CONCLUSIONS

The bidentate N,O-donor **HL** gelator was synthesized and characterized through different spectral techniques. **HL** does not form a gel in aqueous medium, an organic solvent, or in a mixture of solvents; however, the Ni(II) ion triggers it to form **MG** in a THF-MeOH (1:1) binary solvent at room temperature. Different microscopic and spectral analyses, such as SEM, FT-IR, ESI-MS, powder-X-ray diffraction, and rheology analysis, have been used to characterize **MG**. The SEM and PXRD analysis of **MG** revealed a porous spherical-like three-dimensional morphology interconnected with the

Table 2. Charge Conducting Parameters of the MG-based Thin Film Device

device	ϵ_r	μ_{eff} (m^2 V^{-1} s^{-1})	τ (s)	D (m^2 s^{-1})	L_D
MG	1.98	3.25×10^{-6}	5.065×10^{-4}	4.45×10^{-11}	3.18×10^{-7}

https://doi.org/10.1021/acsomega.4c06387
ACS Omega 2025, 10, 378−389

hierarchical arrangements of the self-assembly of the gel network with entirely different structural features of **MG** relative to that of **HL**. The rheological investigation revealed the mechanical and thermal strength of the **MG**. Through this work, we have developed an Ni(II)-selective gel (**MG**) showing good viscoelastic properties as measured through rheological investigations. The mechanical strength and toughness measurements of **MG** enhance its characteristics and may be utilized in diverse engineering and industrial applications. The developed Ni(II)-metallogel **MG**-based Schottky barrier diode exhibits promising diode parameters, indicating the potential of this gel material for future electronic device applications.

■ ASSOCIATED CONTENT

Supporting Information

The Supporting Information is available free of charge at https://pubs.acs.org/doi/10.1021/acsomega.4c06387.

Further information contains about spectral, microscopic, and analytical analysis of **HL** and **MG** in the Figures S1−S11. (PDF)

■ AUTHOR INFORMATION

Corresponding Author

Rampal Pandey − *National Institute of Technology, Uttarakhand, Srinagar (Garhwal) 246174, India; Maulana Azad National Institute of Technology, Bhopal, Bhopal 462003 Madhya Pradesh, India;* orcid.org/0000-0003-1685-7474; Email: rppandeysu@gmail.com

Authors

Vaishali Singh − *National Institute of Technology, Uttarakhand, Srinagar (Garhwal) 246174, India;* orcid.org/0000-0001-7905-0980

Deepak Kumar Chauhan − *Institute of Nano Science and Technology (INST), Mohali 160062, India*

Complete contact information is available at: https://pubs.acs.org/10.1021/acsomega.4c06387

Notes

The authors declare no competing financial interest.

■ ACKNOWLEDGMENTS

The authors are highly obliged to NIT Uttarakhand for providing the chemical supplies and a research laboratory. R.P. is deeply grateful to Maulana Azad National Institute of Technology (MANIT) Bhopal for seed money and financial assistance. V.S. deeply thanks the Ministry of Education (MoE) and NIT Uttarakhand for providing the Institute Fellowship. D.K.C. is deeply grateful to INST Mohali for providing instrumental facilities such as FT-IR, ^{1}H NMR, HRMS, FE-SEM, and powder-XRD analytical techniques.

■ REFERENCES

(1) Kuosmanen, R.; Rissanen, K.; Sievänen, E. Steroidal Supramolecular Metallogels. *Chem. Soc. Rev.* **2020**, *49* (6), 1977−1998.

(2) Wu, H.; Zheng, J.; Kjøniksen, A. L.; Wang, W.; Zhang, Y.; Ma, J. Metallogels: Availability, Applicability, and Advanceability. *Adv. Mater.* **2019**, *31* (12), 1806204.

(3) Kim, T. H.; Kwon, N. Y.; Son, J. H.; Yang, C.; Lee, M.; Lee, T. S. Self-Assembly of Supramolecualr Metallogelator Containing 2-(2'-Hydroxyphenyl) Benzoxazole/Zn(II) Chelate. *J. Nanosci. Nanotechnol.* **2010**, *10* (10), 6929−6933.

(4) Sheikhi, A.; Van De Ven, T. G. M. Trapping It Softly: Ultrasoft Zirconium Metallogels for Macromolecule Entrapment and Reconfiguration. *ACS Macro Lett.* **2016**, *5* (8), 904−908.

(5) Bairagi, D.; Biswas, P.; Basu, K.; Hazra, S.; Hermida-Merino, D.; Sinha, D. K.; Hamley, I. W.; Banerjee, A. Self-Assembling Peptide-Based Hydrogel: Regulation of Mechanical Stiffness and Thermal Stability and 3D Cell Culture of Fibroblasts. *ACS Appl. Bio Mater.* **2019**, *2* (12), 5235−5244.

(6) Martínez-Calvo, M.; Kotova, O.; Möbius, M. E.; Bell, A. P.; McCabe, T.; Boland, J. J.; Gunnlaugsson, T. Healable Luminescent Self-Assembly Supramolecular Metallogels Possessing Lanthanide (Eu/Tb) Dependent Rheological and Morphological Properties. *J. Am. Chem. Soc.* **2015**, *137* (5), 1983−1992.

(7) Kuroiwa, K.; Kimizuka, N. Self-Assembly and Functionalization of Lipophilic Metal-Triazole Complexes in Various Media. *Polym. J.* **2013**, *45*, 384−390.

(8) Bachman, R. E.; Zucchero, A. J.; Robinson, L. J. General Approach to Low-Molecular-Weight Metallogelators via the Coordination-Induced Gelation of an l-Glutamate-Based Lipid. *Langmuir* **2012**, *28* (1), 27−30.

(9) Svobodová, H.; Noponen, V.; Kolehmainen, E.; Sievänen, E. Recent Advances in Steroidal Supramolecular Gels. *RSC Adv.* **2012**, *2* (12), 4985−5007.

(10) Rahim, M. A.; Björnmalm, M.; Suma, T.; Faria, M.; Ju, Y.; Kempe, K.; Müllner, M.; Ejima, H.; Stickland, A. D.; Caruso, F. Metal−Phenolic Supramolecular Gelation. *Angew. Chem., Int. Ed.* **2016**, *55* (44), 13803−13807.

(11) Saha, E.; Mitra, J. Multistimuli-Responsive Self-Healable and Moldable Nickel(II)-Based Gels for Reversible Gas Adsorption and Palladium Sequestration via Gel-to-Gel Transformation. *ACS Appl. Mater. Interfaces* **2019**, *11* (11), 10718−10728.

(12) Chen, J.; Wang, T.; Liu, M. A Hydro-Metallogel of an Amphiphilic l-Histidine with Ferric Ions: Shear-Triggered Self-Healing and Shrinkage. *Inorg. Chem. Front.* **2016**, *3* (12), 1559−1565.

(13) Peng, P.; Li, Y.; Song, W.; Yu, X. Self-Healing Organogels and Hydrogels Constructed by Self-Assembled Bis-Terpyridine Complex with Selective Metal Ions. *Colloids Surf., A* **2020**, *589*, No. 124439.

(14) Tao, X.; Chen, X.; Chen, T.; Du, G.; Wang, Y.; Li, Q. Building Multi-Color Emitters with Tailored Lanthanide-Based Supramolecular Metallogels. *Colloids Surf., A* **2022**, *634*, No. 127910.

(15) Guan, Q. L.; Sun, Y.; Huo, R.; Xin, Y.; Bai, F. Y.; Xing, Y. H.; Sun, L. X. Cu-MOF Material Constructed with a Triazine Polycarboxylate Skeleton: Multifunctional Identify and Microdetecting of the Aromatic Diamine Family (o, m, p-Phenylenediamine) Based on the Luminescent Response. *Inorg. Chem.* **2021**, *60* (4), 2829−2838.

(16) Tam, A. Y. Y.; Yam, V. W. W. Recent Advances in Metallogels. *Chem. Soc. Rev.* **2013**, *42* (4), 1540−1567.

(17) Bhattacharya, S.; Sengupta, S.; Bala, S.; Goswami, A.; Ganguly, S.; Mondal, R. Pyrazole-Based Metallogels Showing an Unprecedented Colorimetric Ammonia Gas Sensing through Gel-to-Gel Transformation with a Rare Event of Time-Dependent Morphology Transformation. *Cryst. Growth Des.* **2014**, *14* (5), 2366−2374.

(18) Sutar, P.; Maji, T. K. Coordination Polymer Gels: Soft Metal-Organic Supramolecular Materials and Versatile Applications. *Chem. Commun.* **2016**, *52* (52), 8055−8074.

(19) Dhibar, S.; Dey, A.; Dey, A.; Majumdar, S.; Ghosh, D.; Ray, P. P.; Dey, B. Development of Supramolecular Semiconducting Mn(II)-Metallogel Based Active Device with Substantial Carrier Diffusion Length. *ACS Appl. Electron. Mater.* **2019**, *1* (9), 1899−1908.

(20) Yu, X.; Wang, Z.; Li, Y.; Geng, L.; Ren, J.; Feng, G. Fluorescent and Electrochemical Supramolecular Coordination Polymer Hydrogels Formed from Ion-Tuned Self-Assembly of Small Bis-Terpyridine Monomer. *Inorg. Chem.* **2017**, *56* (13), 7512−7518.

(21) Jiménez, C. C.; Farfán, N.; Romero-Avila, M.; Rodríguez, M.; Aparicio-Ixta, L.; Ramos-Ortiz, G.; Maldonado, J. L.; Santillan, R.; Magaña-Vergara, N. E.; Ochoa, M. E. Synthesis and Chemical-Optical Characterization of Novel Two-Photon Fluorescent Borinates Derived from Schiff Bases. *J. Organomet. Chem.* **2014**, *755*, 33−40.

(22) Chen, P.; Li, Q.; Grindy, S.; Holten-Andersen, N. White-Light-Emitting Lanthanide Metallogels with Tunable Luminescence and Reversible Stimuli-Responsive Properties. *J. Am. Chem. Soc.* **2015**, *137* (36), 11590−11593.
(23) Joarder, B.; Chaudhari, A. K.; Nagarkar, S. S.; Manna, B.; Ghosh, S. K. Amino Acid Based Dynamic Metal-Biomolecule Frameworks. *Chem. − Eur. J.* **2013**, *19* (34), 11178−11183.
(24) Alam, N.; Sarma, D. Tunable Metallogels Based on Bifunctional Ligands: Precursor Metallogels, Spinel Oxides, Dye and CO2Adsorption. *ACS Omega* **2020**, *5* (28), 17356−17366.
(25) Rezaeian, K.; Khanmohammadi, H.; Dogaheh, S. G. Studies on a Multifunctional Chromo-Fluorogenic Sensor for Dual Channel Recognition of Zn2+ and CN− Ions in Aqueous Media: Mimicking Multiple Molecular Logic Gates and Memory Devices. *New J. Chem.* **2018**, *42*, 2158−2166.
(26) Banerjee, S.; Adarsh, N. N.; Dastidar, P. A Crystal Engineering Rationale in Designing a CdII Coordination Polymer Based Metallogel Derived from a C3 Symmetric Tris-Amide-Tris-Carboxylate Ligand. *Soft Matter* **2012**, *8* (29), 7623−7629.
(27) Baglioni, M.; Domingues, J. A. L.; Carretti, E.; Fratini, E.; Chelazzi, D.; Giorgi, R.; Baglioni, P. Complex Fluids Confined into Semi-Interpenetrated Chemical Hydrogels for the Cleaning of Classic Art: A Rheological and SAXS Study. *ACS Appl. Mater. Interfaces* **2018**, *10* (22), 19162−19172.
(28) Singh, V.; Kala, S.; Rom, T.; Paul, A.; Pandey, R. A Multi-Cation Responsive Ni(II)-Supramolecular Metallogel Mimics as Molecular Keypad Lock via Reversible Fluorescence Switching. *Dalton Trans.* **2023**, *52*, 7088−7103.
(29) Yu, J.; Zhang, C. Fluorescent Sensing for Amines with a Low Detection Limit Based on Conjugated Porous Polymers. *J. Mater. Chem. C* **2020**, *8* (46), 16463−16469.
(30) Berhanu, A. L.; Gaurav; Mohiuddin, I.; Malik, A. K.; Aulakh, J. S.; Kumar, V.; Kim, K. H. A Review of the Applications of Schiff Bases as Optical Chemical Sensors. *TrAC, Trends Anal. Chem.* **2019**, *116*, 74−91.
(31) Sangeetha, N. M.; Maitra, U. Supramolecular Gels: Functions and Uses. *Chem. Soc. Rev.* **2005**, *34* (10), 821−836.
(32) Cao, L.; Wang, P.; Miao, X.; Duan, H.; Wang, H.; Dong, Y.; Ma, R.; Zhang, B.; Wu, B.; Li, X.; Stang, P. J. Diamondoid Frameworks via Supramolecular Coordination: Structural Characterization, Metallogel Formation, and Adsorption Study. *Inorg. Chem.* **2019**, *58* (9), 6268−6275.
(33) Benito, Q.; Fargues, A.; Garcia, A.; Maron, S.; Gacoin, T.; Boilot, J. P.; Perruchas, S.; Camerel, F. Photoactive Hybrid Gelators Based on a Luminescent Inorganic [Cu 4I4] Cluster Core. *Chem. − Eur. J.* **2013**, *19* (47), 15831−15835.
(34) Liu, D.; Liu, H.; Song, B.; Chen, M.; Huang, J.; Wang, J.; Yang, X.; Sun, W.; Li, X.; Wang, P. Terpyridine-Based Metallo-Organic Cages and Supramolecular Gelation by Coordination-Driven Self-Assembly and Host-Guest Interaction. *Dalton Trans.* **2018**, *47* (40), 14227−14232.
(35) Mehdi, H.; Pang, H.; Gong, W.; Dhinakaran, M. K.; Wajahat, A.; Kuang, X.; Ning, G. A Novel Smart Supramolecular Organic Gelator Exhibiting Dual-Channel Responsive Sensing Behaviours towards Fluoride Ion: Via Gel-Gel States. *Org. Biomol. Chem.* **2016**, *14* (25), 5956−5964.
(36) Ma, X.; Cui, Y.; Liu, S.; Wu, J. A Thermo-Responsive Supramolecular Gel and Its Luminescence Enhancement Induced by Rare Earth Y3+. *Soft Matter* **2017**, *13* (44), 8027−8030.
(37) Dietrich, D.; Licht, C.; Nuhnen, A.; Höfert, S. P.; De Laporte, L.; Janiak, C. Metal-Organic Gels Based on a Bisamide Tetracarboxyl Ligand for Carbon Dioxide, Sulfur Dioxide, and Selective Dye Uptake. *ACS Appl. Mater. Interfaces* **2019**, *11* (21), 19654−19667.
(38) Morris, J.; Bietsch, J.; Bashaw, K.; Wang, G. Recently Developed Carbohydrate Based Gelators and Their Applications. *Gels* **2021**, *7*, No. 24, DOI: 10.3390/gels7010024.
(39) Afrasiabi, R.; Kraatz, H. B. Rational Design and Application of a Redox-Active, Photoresponsive, Discrete Metallogelator. *Chem. − Eur. J.* **2015**, *21* (21), 7695−7700.
(40) Sarkar, K.; Dastidar, P. Rational Approach Towards Designing Metallogels From a Urea-Functionalized Pyridyl Dicarboxylate: Anti-Inflammatory, Anticancer, and Drug Delivery. *Chem. − Asian J.* **2019**, *14* (1), 194−204.
(41) Malviya, N.; Sonkar, C.; Kundu, B. K.; Mukhopadhyay, S. Discotic Organic Gelators in Ion Sensing, Metallogel Formation, and Bioinspired Catalysis. *Langmuir* **2018**, *34* (38), 11575−11585.
(42) Kelly, N.; Gloe, K.; Doert, T.; Hennersdorf, F.; Heine, A.; März, J.; Schwarzenbolz, U.; Weigand, J. J.; Gloe, K. Self-Assembly of [2 + 2] Co(II) Metallomacrocycles and Ni(II) Metallogels with Novel Bis(Pyridylimine) Ligands. *J. Organomet. Chem.* **2016**, *821*, 182−191.
(43) Das, P.; Majumdar, S.; Dey, A.; Mandal, S.; Mondal, A.; Chakrabarty, S.; Ray, P. P.; Dey, B. 4,4′-Bipyridine-Based Ni(Ii)-Metallogel for Fabricating a Photo-Responsive Schottky Barrier Diode Device. *New J. Chem.* **2021**, *45* (35), 15920−15927.
(44) Pandey, V. K.; Dixit, M. K.; Manneville, S.; Bucher, C.; Dubey, M. A Multi-Stimuli Responsive Conductive Sonometallogel: A Mechanistic Insight into the Role of Ultrasound in Gelation. *J. Mater. Chem. A* **2017**, *5* (13), 6211−6218.
(45) Ali, R.; Dwivedi, S. K.; Mishra, H.; Misra, A. Imidazole-Coumarin Containing D − A Type Fluorescent Probe: Synthesis Photophysical Properties and Sensing Behavior for F− and CN− Anion. *Dyes Pigm.* **2020**, *175*, No. 108163.
(46) Yao, H.; Niu, Y.; Kan, X.; Hu, Y.; He, Y.; Wei, T.; Zhang, Y.; Lin, Q. Dyes and Pigments Controllable Self-Assemblies of 2, 2 ′ -Bibenzimidazole Derivative: Detection and Adsorption of Heavy Metal Ion. *Dyes Pigm.* **2022**, *198*, No. 110021.
(47) Sitkowski, J.; Stefaniak, L.; Dziembowska, T.; Grech, E.; Jagodzińska, E.; Webb, G. A. A Multinuclear NMR Study of Proton Transfer Processes in Schiff Bases. *J. Mol. Struct.* **1996**, *381* (1−3), 177−180.
(48) Rezaeian, K.; Khanmohammadi, H.; Dogaheh, S. G. Studies on Multifunctional Chromo-Fluorogenic Sensor for Dual Channel Recognition of Zn2+ and $C\bar{N}$ Ions in Aqueous Media: Mimicking Multiple Molecular Logic Gates and Memory Devices. *New J. Chem.* **2018**, *42*, 2158.
(49) Rudkevich, D. M. Intramolecular Hydrogen Bonding in Calixarenes. *Chem. − Eur. J.* **2000**, *6* (15), 2679−2686.
(50) Panja, A.; Ghosh, K. Azo and Imine Functionalized 2-Naphthols: Promising Supramolecular Gelators for Selective Detection of Fe3+ and Cu2+, Reactive Oxygen Species and Halides. *Mater. Chem. Front.* **2018**, *2* (10), 1866−1875.
(51) Panja, S.; Adams, D. J. Stimuli Responsive Dynamic Transformations in Supramolecular Gels. *Chem. Soc. Rev.* **2021**, *50* (8), 5165−5200.
(52) Singh, V.; Dwivedi, A. D.; Pandey, R. Anticounterfeiting Feature of a Writable and Self-Erasable Ni(II)-Metallogel Pad via Fluorescent "Turn-On" Detection of Cyanide. *Langmuir* **2024**, *40* (10), 5121−5136.
(53) Singh, V.; Srivastava, A.; Pandey, M. D.; Pandey, R. Ni(II)/Yb(III)-Metallogels for Distinctive Fluorescent 'Turn-on' Detection of m-Phenylenediamine: Toward Construction of Multiple Logic Gates. *J. Photochem. Photobiol. A* **2025**, *459*, No. 116003.
(54) Basu, U.; Pant, I.; Hussain, A.; Kondaiah, P.; Chakravarty, A. R. Iron(III) Complexes of a Pyridoxal Schiff Base for Enhanced Cellular Uptake with Selectivity and Remarkable Photocytotoxicity. *Inorg. Chem.* **2015**, *54* (8), 3748−3758.
(55) Kurbah, S. D.; Lal, R. A. Bioinspired Catalysis and Bromoperoxidase like Activity of a Multistimuli-Responsive Supramolecular Metallogel: Supramolecular Assembly Triggered by Pi-Pi Stacking and Hydrogen Bonding Interactions. *New J. Chem.* **2020**, *44* (14), 5410−5418.
(56) Bhattacharjee, S.; Maiti, B.; Bhattacharya, S. First Report of Charge-Transfer Induced Heat-Set Hydrogel. Structural Insights and Remarkable Properties. *Nanoscale* **2016**, *8* (21), 11224−11233.
(57) Tam, A. Y. Y.; Wong, K. M. C.; Zhu, N.; Wang, G.; Yam, V. W. W. Luminescent Alkynylplatinum(II) Terpyridyl Metallogels Stabi-

lized by Pt ···Pt, π-π and Hydrophobic-Hydrophobic Interactions. *Langmuir* **2009**, *25* (15), 8685−8695.
(58) He, T.; Li, K.; Wang, N.; Liao, Y. X.; Wang, X.; Yu, X. Q. A Ferrocene-Based Multiple-Stimuli Responsive Organometallogel. *Soft Matter* **2014**, *10* (21), 3755−3761.
(59) Adarsh, N. N.; Dastidar, P. A New Series of ZnII Coordination Polymer Based Metallogels Derived from Bis-Pyridyl-Bis-Amide Ligands: A Crystal Engineering Approach. *Cryst. Growth Des.* **2011**, *11* (1), 328−336.
(60) Dixit, M. K.; Dubey, M. Li+-Induced Fluorescent Metallogel: A Case of ESIPT-CHEF and ICT Phenomenon. *Phys. Chem. Chem. Phys.* **2018**, *20* (36), 23762−23772.
(61) Malviya, N.; Sonkar, C.; Ganguly, R.; Mukhopadhyay, S.; Kundu, B. K.; Mukhopadhyay, S. Discotic Organic Gelators in Ion Sensing, Metallogel Formation, and Bioinspired Catalysis. *J. Appl. Crystallogr.* **2019**, *48* (1), 7501−7503.
(62) Zhou, Z.; Yan, X.; Cook, T. R.; Saha, M. L.; Stang, P. J. Engineering Functionalization in a Supramolecular Polymer: Hierarchical Self-Organization of Triply Orthogonal Non-Covalent Interactions on a Supramolecular Coordination Complex Platform. *J. Am. Chem. Soc.* **2016**, *138* (3), 806−809.
(63) Kotova, O.; Daly, R.; Dos Santos, C. M. G.; Kruger, P. E.; Boland, J. J.; Gunnlaugsson, T. Cross-Linking the Fibers of Supramolecular Gels Formed from a Tripodal Terpyridine Derived Ligand with d-Block Metal Ions. *Inorg. Chem.* **2015**, *54* (16), 7735−7741.
(64) Knichal, J. V.; Gee, W. J.; Burrows, A. D.; Raithby, P. R.; Wilson, C. C. A New Small Molecule Gelator and 3D Framework Ligator of Lead(II). *CrystEngComm* **2015**, *17* (42), 8139−8145.
(65) Liu, K.; Meng, L.; Mo, S.; Zhang, M.; Mao, Y.; Cao, X.; Huang, C.; Yi, T. Colour Change and Luminescence Enhancement in a Cholesterol-Based Terpyridyl Platinum Metallogel via Sonication. *J. Mater. Chem. C* **2013**, *1* (9), 1753−1762.
(66) Saravanan, T.; Anandan, P.; Shanmugam, M.; Azhagurajan, M.; Mohamed Ismail, M.; Arivanandhan, M.; Hayakawa, Y.; Jayavel, R. Facile Synthesis of Yb2O3−Graphene Nanocomposites for Enhanced Energy and Environmental Applications. *Polym. Bull.* **2020**, *77* (8), 3891−3906.
(67) Dhibar, S.; Dey, A.; Jana, R.; Chatterjee, A.; Das, G. K.; Ray, P. P.; Dey, B. A Semiconducting Supramolecular Co(Ii)-Metallohydrogel: An Efficient Catalyst for Single-Pot Aryl-S Bond Formation at Room Temperature. *Dalton Trans.* **2019**, *48* (46), 17388−17394.
(68) Tang, S.; Olsen, B. D. Relaxation Processes in Supramolecular Metallogels Based on Histidine-Nickel Coordination Bonds. *Macromolecules* **2016**, *49* (23), 9163−9175.
(69) Fang, W.; Sun, Z.; Tu, T. Novel Supramolecular Thixotropic Metallohydrogels Consisting of Rare Metal-Organic Nanoparticles: Synthesis, Characterization, and Mechanism of Aggregation. *J. Phys. Chem. C* **2013**, *117* (47), 25185−25194.
(70) Tuncaboylu, D. C.; Sari, M.; Oppermann, W.; Okay, O. Tough and Self-Healing Hydrogels Formed via Hydrophobic Interactions. *Macromolecules* **2011**, *44* (12), 4997−5005.
(71) Sallee, A.; Ghebreyessus, K. Photoresponsive Zn2+-Specific Metallohydrogels Coassembled from Imidazole Containing Phenylalanine and Arylazopyrazole Derivatives. *Dalton Trans.* **2020**, *49* (30), 10441−10451.
(72) Dixit, M. K.; Pandey, V. K.; Dubey, M. Alkali Base Triggered Intramolecular Charge Transfer Metallogels Based on Symmetrical A-π-D-Chiral-D-π-A Type Ligands. *Soft Matter* **2016**, *12* (15), 3622−3630.
(73) Dubey, M.; Kumar, A.; Kumar Gupta, R.; Shankar Pandey, D. Li+-Induced Selective Gelation of Discrete Homochiral Structural Isomers Derived from l-Tartaric Acid. *Chem. Commun.* **2014**, *50* (51), 8144−8147.
(74) Boul, P. J.; Jarowski, P. D.; Thaemlitz, C. J. Phase Change Transformations with Dynamically Addressable Aminal Metallogels. *J. Am. Chem. Soc.* **2017**, *139* (43), 15385−15391.
(75) Zhang, M.; Weiss, R. G. Mechano-Switchable, Luminescent Gels Derived from Salts of a Long-Chained, Fatty-Acid Gelator. *Phys. Chem. Chem. Phys.* **2016**, *18* (30), 20399−20409.
(76) Mahendar, C.; Kumar, Y.; Dixit, M. K.; Dubey, M. An Li+-Enriched Co2+-Induced Metallogel: A Study on Thixotropic Rheological Behaviour and Conductance. *Soft Matter* **2020**, *16* (14), 3436−3442.
(77) Özkınalı, S.; Gür, M.; Şener, N.; Alkın, S.; Çavuş, M. S. Synthesis of New Azo Schiff Bases of Pyrazole Derivatives and Their Spectroscopic and Theoretical Investigations. *J. Mol. Struct.* **2018**, *1174*, 74−83.
(78) Issa, R. M.; Khedr, A. M.; Rizk, H. F. UV-Vis, IR and 1H NMR Spectroscopic Studies of Some Schiff Bases Derivatives of 4-Aminoantipyrine. *Spectrochim. Acta, Part A* **2005**, *62* (1−3), 621−629.
(79) Issa, R. M.; Khedr, A. M.; Rizk, H. H NMR, IR and UV/VIS Spectroscopic Studies of Some Schiff Bases Derived from 2-Aminobenzothiazole and 2-Amino-3-Hydroxypyridine. *J. Chin. Chem. Soc.* **2008**, *55* (4), 875−884.
(80) Konar, S.; Jana, A.; Das, K.; Ray, S.; Chatterjee, S.; Golen, J. A.; Rheingold, A. L.; Kar, S. K. Synthesis, Crystal Structure, Spectroscopic and Photoluminescence Studies of Manganese(II), Cobalt(II), Cadmium(II), Zinc(II) and Copper(II) Complexes with a Pyrazole Derived Schiff Base Ligand. *Polyhedron* **2011**, *30* (17), 2801−2808.
(81) Kusmariya, B. S.; Tiwari, A.; Mishra, A. P.; Naikoo, G. A. Theoretical and Experimental Studies of Cu(II) and Zn(II) Coordination Compounds with N,O Donor Bidentate Schiff Base Ligand Containing Amino Phenol Moiety. *J. Mol. Struct.* **2016**, *1119*, 115−123.
(82) Dhibar, S.; Dey, A.; Majumdar, S.; Ghosh, D.; Mandal, A.; Ray, P. P.; Dey, B. A Supramolecular Cd(Ii)-Metallogel: An Efficient Semiconductive Electronic Device. *Dalton Trans.* **2018**, *47* (48), 17412−17420.
(83) Dey, A.; Sil, S.; Majumdar, S.; Sahu, R.; Ghosh, M.; Lepcha, G.; Ray, P. P.; Dey, B. Exploring the Studies of Charge Transportation of an Aromatic Acid Based Co(II)-Metallogel Scaffold Fabricated Schottky Device. *J. Phys. Chem. Solids* **2022**, *160*, No. 110300.
(84) Dhibar, S.; Dey, A.; Majumdar, S.; Ray, P. P.; Dey, B. Terephthalic Acid-Directed Supramolecular Cu(II)-Metallogel for Photosensitive Semiconducting Schottky Diode with Promising Electronic Charge Transportation. *Int. J. Energy Res.* **2021**, *45* (4), 5486−5499.
(85) Kumar, V.; Upadhyay, R. K.; Bano, D.; Chandra, S.; Kumar, D.; Jit, S.; Hasan, S. H. The Fabrication and Characterization of a Supramolecular Cu-Based Metallogel Thin-Film Based Schottky Diode. *New J. Chem.* **2021**, *45* (14), 6273−6280.
(86) Dhibar, S.; Dey, A.; Dey, A.; Majumdar, S.; Mandal, A.; Ray, P. P.; Dey, B. The Development of a Rapid Self-Healing Semiconducting Monoethanolamine-Based Mg(OH)2 Metallogel for a Schottky Diode Application with a High ON/OFF Ratio. *New J. Chem.* **2019**, *43* (39), 15691−15699.
(87) Dhibar, S.; Dey, A.; Majumdar, S.; Dey, A.; Ray, P. P.; Dey, B. Organic-Acid-Mediated Luminescent Supramolecular Tb(III)-Metallogel Applied in an Efficient Photosensitive Electronic Device with Excellent Charge Transport Properties. *Ind. Eng. Chem. Res.* **2020**, *59* (13), 5466−5473.
(88) Majumdar, S.; Sil, S.; Sahu, R.; Ghosh, M.; Lepcha, G.; Dey, A.; Mandal, S.; Pratim Ray, P.; Dey, B. Electronic Charge Transport Phenomena Directed Smart Fabrication of Metal-Semiconductor Based Electronic Junction Device by a Supramolecular Mn(II)-Metallogel. *J. Mol. Liq.* **2021**, *338*, No. 116769.
(89) Dhibar, S.; Dey, A.; Ghosh, D.; Majumdar, S.; Dey, A.; Ray, P. P.; Dey, B. Triethylenetetramine-Based Semiconducting Fe(III) Metallogel: Effective Catalyst for Aryl-S Coupling. *ACS Omega* **2020**, *5* (6), 2680−2689.

https://doi.org/10.1021/acsomega.4c06387
ACS Omega 2025, 10, 378−389